Environmental Science Nano

Antifouling Properties of Two Dimensional Molybdenum Disulfide and Graphene Oxide Nanomaterials

Journal:	*Environmental Science: Nano*
Manuscript ID	EN-ART-02-2018-000202.R1
Article Type:	Paper
Date Submitted by the Author:	26-Apr-2018

Complete List of Authors:	Alam, Iftaykhairul; Washington State University, Civil and Environmental Engineering Guiney, Linda; Northwestern University, Department of Materials Science and Engineering Hersam, Mark; Northwestern University, Department of Materials Science and Engineering Chowdhury, Indranil; Washington State University,

Environmental Significant Statement

Two-dimensional graphene-based nanomaterials including graphene oxide (GO) and reduced graphene oxide (rGO) have shown antibacterial properties, which could be useful for different environmental applications. Many studies also reported the potential application of GO/rGO for antifouling membrane preparation. While graphene-based materials have been extensively studied, recently molybdenum disulfide (MoS_2) nanosheets have gained lot of attentions. Most of the research that has focused on MoS_2 for application in electronics, catalysis, biomedical and energy related fields. However, its use as an antifouling material has not been extensively explored. MoS_2 has extremely low friction as well as low surface roughness and so MoS_2 has great potential for antifouling surface preparation. Overall MoS_2 showed superior antifouling properties compared to GO in this study. Results indicate that MoS_2 may be more suitable for antifouling surfaces in environmental applications. Integration of MoS_2 for the preparation of antifouling surface could be applied in different industries such as water filters, ship hulls, biomedical devices, coatings, and paintings.

Antifouling Properties of Two Dimensional Molybdenum Disulfide and Graphene Oxide

Iftaykhairul Alam [1], Linda M. Guiney[2], Mark C. Hersam[2], and Indranil Chowdhury [1*]

[1] Department of Civil & Environmental Engineering, Washington State University, Pullman, WA 99164, USA

[2] Departments of Materials Science and Engineering, Chemistry, and Medicine, Northwestern University, Evanston, Illinois 60208, USA

*Contacting author: indranil.chowdhury@wsu.edu; 509-335-3721

Abstract

Fouling remains one of the biggest challenges in a myriad of industries such as water filters, ship hulls, biomedical devices, coatings, and paintings. Fouling severely hampers the performance and increase the operation and maintenance costs in industries. There is a critical need to develop antifouling surfaces and two-dimensional (2D) materials, such as graphene oxide (GO) and molybdenum disulfide (MoS_2), have shown potential for antifouling surface preparation due to some unique properties. Here, the antifouling properties of these two materials were investigated by observing the deposition kinetics of bacteria and natural organic matter (NOM) using a quartz crystal microbalance with dissipation monitoring (QCM-D). Suwannee River humic acid (SRHA) and *E. coli* K-12 were used as model NOM and bacteria, respectively. Overall MoS_2 showed slightly better antifouling properties compared to GO. In most cases, the deposition of NOM and *E. coli* was significantly lower on MoS_2 than GO due to the presence of functional groups on GO that bind more easily with the foulants. Deposition of NOM was at least 1.5 times lower on MoS_2 surface than GO surface in the presence of both monovalent (Na^+) and divalent (Mg^{2+}) cations. However, the presence of 0.5 mM divalent cations (Ca^{2+}, Mg^{2+}) with NOM reduced the antifouling properties of both MoS_2 and GO by a factor of $\geq$1.5 due to a salt bridging effect and reduced energy barrier.

1. Introduction

Two-dimensional graphene-based nanomaterials including graphene oxide (GO) and reduced graphene oxide (rGO) have shown great potential in different environmental applications such as photocatalytic oxidation, contaminant removal, membrane-based separation etc. [1-3] Several studies have demonstrated the strong antimicrobial properties of GO against a wide variety of microorganisms, including gram-positive and gram-negative bacterial pathogens, phyto-pathogens, and biofilm-forming microorganisms.[4, 5] Additionally, GO is hydrophilic, which could result in higher water permeation, making the membrane less susceptible to fouling during filtration.[6, 7] While graphene-based materials have been extensively studied, recently molybdenum disulfide (MoS_2) nanosheets have gained lot of attentions. MoS_2, a member of the emerging 2D nanomaterial class of transition metal dichalcogenides, has unique electrical, physicochemical and mechanical properties. [8, 9] Despite the significant research that has focused on MoS_2 for application in electronics, catalysis, biomedical and energy related fields, its use as an antifouling material has not been extensively explored. MoS_2 has extremely low friction and low surface roughness.[10, 11] Foulants are less likely to adhere to the MoS_2 surfaces due to this property.[12, 13] The advancement of membrane technology for water filtration is severely hampered by the long-standing problem of fouling, which is caused by the accumulation of foreign substances on the membrane surfaces or inside the membrane pores.[14, 15] Fouling has been found to deteriorate membrane performance causing low water permeability, poor product water quality, high energy consumption, and short membrane life. [16, 17] Biofouling, colloidal fouling, organic fouling and scaling remain the most significant problems for efficient application of nano-filtration and reverse osmosis.[18, 19] Beside fouling in water filtration membrane, fouling also causes serious problem in marine ship hulls due to the presence of more

than 4000 species of marine organisms.[20-22] Fouling by different proteins and bacteria has also been reported in biomedical applications, including biosensors, bioanalytical devices, and implants. [23, 24]

Before integrating MoS_2 for the preparation of antifouling surface into water filtration membranes or biomedical devices, it is important to understand the antifouling mechanisms of this nanomaterial. In this work, the antifouling performance of MoS_2 and GO has been compared in terms of maximum foulants deposition and foulants deposition rates on those material surfaces. A quartz crystal microbalance with dissipation monitoring (QCM-D) was used to study the interactions of MoS_2 and GO with natural organic matter (NOM) and *E. coli* (K-12). NOM is mainly composed of humic substances and polysaccharides and is common in the aquatic environment.[25] *E. coli* K12 is also common in natural water and one of the most commonly used bacteria strains for fouling studies. [26, 27] Interaction of these foulants with MoS_2 and GO will thus give a clear indication of the antifouling properties of the materials. The impact of ion presence and valence on the attachment of foulants with MoS_2 and GO is also investigated.

2. Materials and Methods

2.1 Preparation of materials

2D GO and MoS_2 were both synthesized using top-down approaches. A modified Hummers' method was used to synthesize graphene oxide.[28, 29] Detailed synthesis process of GO is provided in the supporting information. The MoS_2 nanomaterial used in this study was synthesized using a lithiation process described elsewhere.[30] Briefly, Lithium intercalation was achieved by combining bulk MoS_2 powder and butyllithium in a low vapor and oxygen condition for 2 days with continuous stirring. The lithiated MoS_2 was rinsed extensively with hexane, filtered, and

exfoliated by the addition of deionized water and bath sonication. The resulting dispersion was centrifuged to remove any unexfoliated material. The supernatant was further dialyzed for 7 days in a bath of deionized water to remove residual lithium and hexane.

2.2 Characterization of materials

AFM imaging was used to determine the surface roughness of the materials. X-ray photoelectron spectroscopy (XPS) was done to determine the amount of functional groups present in GO and MoS_2 materials. Hydrodynamic diameter (D_h) and zeta potential (ζ-potential) of the materials and the *E. coli* were also measured for the calculation of DLVO theory (supporting information). Contact angle measurement also done to determine the hydraphilicity of GO and MoS_2.

2.2.1 AFM and XPS analysis

The surface roughness of GO, MoS_2 and PLL were measured by atomic force microscopy (AFM) using a similar procedure on previously published work.[28, 29] Si wafers with a 100 nm thick oxide surface were used as substrates. At first, Si wafers were washed by acetone and isopropanol, and then rinsed with deionized (DI) water. For preparing a self-assembled functionalized monolayer, the Si wafers were put in a 2.5 mM (3- amino propyl) triethoxysilane (APTES) solution for 30 minutes and then rinsed with DI water again. Then immediately after drying with N_2, a 5 mg/L GO/MoS_2/PLL drop was placed on the surface. After waiting for 10 min, the sample was rinsed with DI water and dried with N_2. The sample was further heat treated at 250°C for 30 min for removing the residual APTES. AFM images were taken using a Thermo Microscopes Auto probe CP-Research AFM in tapping mode with conical, symmetric probes (Budget Sensors, All-In-One, cantilever B). Images were taken at several random locations on each sample and showed little variation.

Samples for XPS analysis were prepared using a procedure similar to previously published work. [31] XPS samples (approximately 5 mg) were prepared by vacuum filtration of the material dispersions onto a PTFE membrane filter with a 0.1 μm pore size (Millipore). The film was allowed to settle for 15 minutes, rinsed with 30 mL DI water, and allowed to dry in air. XPS spectra were collected using a Thermo Scientific ESCALAB 250Xi. XPS spectra were then corrected for background and fitted for peaks manually.

2.2.2 Electrokinetic and Hydrodynamic Characterization

Hydrodynamic diameter (D_h) and zeta potential (ζ-potential) were measured using a Zeta Sizer Nano ZS (Malvern Instruments, Worcestershire, U.K.), following well-established techniques.[29] [30, 32] ZetaSizer Nano ZS was equipped with a monochromatic coherent He-Ne laser with a fixed wavelength of 633 nm. ZetaSizer Nano ZS uses the Stokes−Einstein equation to calculate the intensity averaged (average size) hydrodynamic diameter (D_h). [33] Zeta potentials (ζ-potential) of the GO, MoS_2 and *E. coli* were also measured using a ZetaSizer Nano ZS instrument, which employs phase analysis light scattering (PALS) to measure the electrophoretic mobility of charged particles. [34] ZetaSizer Nano ZS uses the Smoluchowski equation to calculate ζ-potential from electrophoretic mobility (EPM). [33]

2.2.3 Contact angle measurement

25 μL of GO and MoS_2 dispersions at a concentration of 0.02 mg mL^{-1} was drop cast onto a clean SiO_2 wafer. A 5 μL water droplet was placed onto the surface and the contact angle was measured within 30 seconds using a Krüss DSA100 Drop Size Analyzer. Error bars represent one standard deviation (n = 3).

2.3 Aquatic chemistry

Suwannee River humic acid (Standard II, International Humic Substances Society) was used to prepare the natural organic matter (NOM) suspension at a concentration of 10 mg/L. *Escherichia coli* (*E. coli,* MG1655, K-12) was supplied by the *E. coli* Genetic Resource Center of Yale University. GO or MoS_2 surfaces on gold crystals for QCM-D measurements were prepared by modifying the gold sensors with cationic Poly-L-lysine hydrobromide (PLL, molecular weight 70 000−150 000 Da by viscosity, P-1274, Sigma Aldrich, St. Louis, MO). PLL was dissolved in HEPES buffer (pH 7.4) made from 10 mM *N*-(2-hydroxyethyl) piperazine-*N*-2-ethanesulfonic acid (Sigma), 100 mM NaCl and deionized water and was stored at 4 °C. The final concentration of the stock PLL solution was 0.1 g L^{-1}. The gold substrate cells were exposed to the PLL stock solution for 15-20 min to create a homogeneous layer. Calcium chloride ($CaCl_2.2H_20$, CAS 10035048), sodium chloride (NaCl, CAS 7647-14-5) and magnesium chloride ($MgCl_2.6H_20$, CAS: 7791-18-6) were used to prepare salt solutions. 10 mM NaCl and 0.5 mM $CaCl_2/MgCl_2$ were used for the experiments. 10 mg/L GO and 50 mg/L MoS_2 were prepared from the stock sample solutions.

2.4 Bacterial Strains and Growth Studies

Escherichia coli MG1655 used in this study was pre-cultured, cultured and then harvested following the standard procedure.[35] First, a sterile tip was used to pick up bacteria from the petri dish, after which the tip with bacteria was stirred in 5 mL of lysogeny broth (LB-Miller). Then it was incubated overnight at 37 °C. To culture, 2 mL of pre-culture was added to 200 mL of fresh LB broth and incubated for 24 hr at 37 °C to reach the stationary phase of the bacterial cells. For

harvesting, 40 mL of culture liquid was poured into a centrifuge tube and then centrifuged at 3689 g for 15 min at 4 °C. The supernatant was discarded and the pellet was resuspended by adding 10 mL of 10 mM NaCl and vortexing. Then it was again centrifuged at 3689 g for 15 min at 4 °C and the same procedure was followed to resuspend the pellet in 10 mM NaCl. The cell concentration used in this study was ~10^6 cells per mL. The final cell suspensions were made in the background solution (10 mM Na^+ or 0.5mM Ca^{2+}).

2.5 Fouling study

2.5.1 Foulant deposition with nanomaterial coated surface

Gold sensors were coated with the nanomaterial of interest using the same procedure from previous studies (Fig. S1).[29, 36] Briefly, to achieve a stable baseline reading, the gold sensor surface was rinsed with milli-Q (MQ) water until the changes in frequency and dissipation were <0.3 Hz and <0.2*10^{-6} respectively for 10 min. (Stage I).[37] The QCM-D system was equilibrated with HEPES buffer in 100 mM NaCl solution for 30 min at a flow rate of 0.1 mL/min (Stage II). PLL in HEPES buffer solution was introduced at 0.1 mL/min (Stage III). The PLL layer was rinsed with HEPES for 20 min to remove the unadsorbed PLL (Stage IV). Finally, 1 mM NaCl solution (background electrolyte) was used to remove the buffer at a flow rate of 0.1 mL/min for 30 min (Stage V). 10 mg/L GO or 50 mg/L MoS_2 was deposited on the PLL coated surface by flowing at a rate of 0.1 mL/min for at least 30 min (Stage VI). Similar type of approach was used to deposit nanomaterials on QCM-D sensors in previous studies. [36, 37] MoS_2 showed slow deposition on PLL and thus a higher concentration of MoS_2 was employed to achieve a fully coated sensor in a reasonable time period. The sensors were exposed to the GO and MoS_2 solutions until maximum frequency was achieved and the frequency shift became stable indicating full coverage of both materials on the PLL surface. All the fouling experiments were

done on bare PLL surface also to compare the results with the GO/MoS_2 coated surface (Fig. S2). This was done to confirm that no PLL was exposed during the fouling study and the foulants only interacted with GO and MoS_2 surfaces. Any exposed PLL even after GO/MoS_2 coating would result into higher frequency shifts and dissipation changes like bare PLL surface experiment.To test the antifouling properties, NOM and *E. coli* were injected across the nanomaterial-coated surface at a flow rate of 0.1 mL/min until the QCM-D showed a stable frequency shift. QCM-D cells and sensors were cleaned following the Q-sense cleaning protocols before and after the experiment. Briefly, 5 mL of Hellmanex III (Fisherbrand ™, cleaning concentrate) was flowed through the tubes to the QCM-D cells followed by 20 mL of Milli-Q water to clean the cells. The gold sensors were soaked in a solution of 5:1:1 Milli-Q water, NH_4OH and H_20_2 at 75 ± 5 °C for 5 min. The sensors were air dried and placed in a UV chamber for 20 min. All the fouling study were replicated three times and results are summarized in table S1.

2.5.2 Deposition and release study using QCM-D

The deposition kinetics of NOM and *E. coli* were determined from the frequency shifts monitored by QCM-D from which the deposition rate and attachment efficiency can be calculated.[38] Shifts in frequency and dissipation were monitored at the third overtone. Initial deposition rates r_f and r_D are defined as rates of frequency and dissipation shift in a time period respectively (Eq. 1 and 2) [36, 39]:

$$r_f = \left|\left(\frac{d\Delta f_{(3)}}{dt}\right)_{t\to 0}\right| \quad (1)$$

$$r_D = \left|\left(\frac{d\Delta D_{(3)}}{dt}\right)_{t\to 0}\right| \quad (2)$$

Attachment efficiency gives information on how fast the foulants deposit on the material surface with respect to bare polymer surfaces (PLL). [36, 39] It is a good indicator for comparing the antifouling performance of GO and MoS_2. The deposition attachment efficiency (α_D) is calculated from deposition rates:

$$\alpha_D = \frac{r_f}{(r_f)\text{PLL}} = \frac{\left|\left(\frac{d\Delta f_{(3)}}{dt}\right)_{t\to 0}\right|}{\left|\left(\frac{d\Delta f_{(3)}}{dt}\right)_{\text{PLL},\ t\to 0}\right|} \quad (3)$$

NOM and *E. coli* were directly deposited on PLL surfaces as a control to investigate the deposition behavior of foulants. In Eq. 3, the denominator represents the rate of frequency shift obtained with bare polymer surface conditions. An attachment efficiency of <1 indicates the slower foulant deposition rate on the surfaces functionalized with GO or MoS_2 when compared to a bare polymer surface, which is expected as PLL is positively charged and most likely to interact more with negatively charged foulants. Attachment efficiencies of foulants on GO and MoS_2 were calculated using Eq. 3 and then the antifouling performance of GO and MoS_2 was directly compared.

3. Results and discussion

3.1 Characterization of GO and MoS_2

The average hydrodynamic diameters (Table 1) of GO and MoS_2 in deionized water were 385.3 ± 7.58 nm and 153.5 ± 1.67 nm, respectively. Zeta potentials (Table 1) of GO and MoS_2 in deionized water were -41.33 ± 0.5 mV and -40.34 ± 0.76 mV, respectively. The highly negative zeta potentials of MoS_2 and GO indicate that they are moderately stable in water. Additionally, this suggests that MoS_2 and GO functionalized surfaces could effectively repel foulants due to

the negative surface charge of most foulants.[37] Representative atomic force microscopy (AFM) images of GO and MoS_2 are shown in figure 1. The surface roughness of the GO and MoS_2 on PLL coated gold sensors were 2.5 ± 0.3 nm and 2.4 ± 0.3 nm, respectively. The surface roughness of a bare PLL surface was found to be 5.1 ± 1.2 nm. From these measurements it is clear that the deposition of the 2D materials reduced the roughness of the polymer surface. XPS spectra (Fig. 2) of GO C1s showed three convoluted peaks corresponding to C-C (~284.8 eV), C-O (~286.8 eV) and O-C=O (288.5 eV). For MoS_2 three characteristic peaks were seen in the Mo3d scan corresponding to the Mo3d 3/2 (~232.5 eV), Mo3d 5/2 (~229 eV) and S2s (~226.5 eV) and the characteristic doublet peak in the S2p spectrum. These XPS data confirm that there was no oxygen containing functional groups in MoS_2 structure. Contact angle measurement results (Fig. S3) confirms both GO and MoS_2 used in this study were hydrophilic. GO had an contact angle of 25± 5.4 while the contact angle of MoS_2 was 42±4.6 suggesting GO was slightly more hydrophilic than the MoS_2.

3.2 Deposition kinetics of natural organic matter (NOM) on GO and MoS_2 surfaces

The maximum frequency shift on QCM-D was used to determine the maximum deposition of NOM on both surfaces under experimental condtions. The maximum deposition, thus, is an indication of the fouling caused by NOM on GO and MoS_2 surfaces. Following injection of NOM onto the nanomaterial functionalized surfaces, a slight frequency shift was observed on the GO surface (<1.5 Hz), and even less frequency shift was observed on the MoS_2 surface, indicating that MoS_2 will be less prone to fouling from NOM (Fig. 3A, S3, S4). In fact, the change in frequency shift during NOM deposition on MoS_2 is negligible (Fig. S4) as small frequency shift (~0.5 Hz) could be observed due to vibration on the gold sensor. Due to the high zeta potential of GO and MoS_2 and negative charge of NOM, the interaction of NOM with the

material surfaces will be minimal due to electrostatic repulsion, and thus there is hardly any deposition of NOM on the material surfaces.

NOM attaches to a GO and MoS_2 functionalized surfaces 70% and 80% more slowly on average than a bare polymer surface (favorable condition) respectively (Fig. 3B), suggesting NOM depsoits on both the surfaces at a similar rate. However, less NOM attachment makes MoS_2 preferable to GO as an antifouling surface. These results agree with previous studies which have shown that interactions between GO surfaces and NOM are electrostatically unfavorable[39] as NOM is negatively charged under environmentally relevant conditions.[40] No significant deposition of NOM was observed on the MoS_2 surface despite a zeta potential similar to GO. The difference in their interactions with NOM is most likely due to the presence of functional groups on GO that can interact with NOM. Previously it has been shown that GO deposits more readily on surfaces that have been coated with NOM due to the high amount of hydroxyl and carboxyl functional groups on GO that readily bind with functional groups of NOM.[39] Lack of functional groups on MoS_2 may be responsible for lower interactions with NOM.

3.3 Interactions of GO and MoS_2 with natural organic matter (NOM) in the presence of monovalent ions

The maximum shift observed was 1.65 Hz on the GO surface and 1.52 Hz on the MoS_2 surface (Fig. 4A, S6, S7). Though the frequency shifts were not significantly different, the initial deposition rate of NOM in the presence of Na^+ was 0.98 Hz/min (Fig. S6) on a GO surface and 0.64 Hz/min (Fig. S7) on an MoS_2 surface. Using this deposition rate, the attachment efficiencies (Fig. 4B) of NOM were found to be 57% and 36% on GO and MoS_2 surfaces, respectively, indicating that NOM deposits on MoS_2 more slowly than on GO. The slower deposition rate of NOM on MoS_2 makes it a more advantageous material choice than GO for antifouling

properties. The increase in the overall deposition of NOM in this case is mainly due to reduced electrostatic repulsion and the effect of charge neutralization caused by the presence of Na^+ ions. In particular, in the presence of Na^+, the energy barrier between NOM and the material surfaces is reduced, allowing the functional groups of NOM to attach to the material surfaces. In the presence of NaCl, increased interactions between carbon-based nanomaterials with NOM were found in other studies.[37, 41] The increased frequency shift and higher attachment efficiency of NOM in Na^+ to the GO and MoS_2 surfaces clearly indicate that Na^+ certainly plays a role in the deposition of NOM.

3.4 Interactions of GO and MoS_2 with natural organic matter (NOM) in the presence of divalent cations

From the values of maximum frequency shift, it is clear that the deposition of NOM on both material surfaces in the presence of divalent cations is higher than in the presence of monovalent ions (Fig. S8, S9). The average maximum shifts observed for NOM in Ca^{2+} were 5.97 Hz (Fig. S8) and 5.37 Hz (Fig. S9) on GO and MoS_2, respectively, and in Mg^{2+} the maximum frequency shifts were 4.60 Hz and 3.81 Hz on GO and MoS_2, respectively, (Fig. 5A). The average attachment efficiencies (Fig. 5B) of NOM in the presence of Ca^{2+} were 66% and 41% on GO and MoS_2 surfaces, respectively. The attachment efficiencies of NOM in Mg^{2+} were 73% and 39% on GO and MoS_2 surfaces, respectively indicating the superior antifouling properties of MoS_2 over GO (Fig. 5B). The difference in antifouling performance between GO and MoS_2 was more significant in case of NOM in Mg^{2+}. On the other hand, Ca^{2+} in NOM caused the fouling on both GO and MoS_2 surfaces at a similar rate. Moreover,, increased values of both maximum frequency shifts and attachment efficiencies suggest that electrostatic repulsion between the NOM and the GO or MoS_2 surface is reduced in the presence of Ca^{2+} or Mg^{2+}. This decrease in

the energy barrier between NOM and the surface allows the NOM to come into close contact with the material surfaces in the presence of divalent cations. This higher deposition of NOM can also be attributed to salt bridging caused by the divalent cations. This bridging effect is well documented in the literature.[42, 43] Chen and Elimelech observed a slightly higher interaction of fullerenes and Suwannee River humic acid (SRHA) on bare silica in the presence of $CaCl_2$ due to SRHA macromolecules undergoing complex formation with Ca^{2+} that reduces electrostatic and steric effects.[37] Chowdhury et al. found a similar bridging effect of divalent cations during the interaction of GO and Suwannee River fulvic acid (SRFA) using QCM-D.[39] It is clear from this study that the antifouling ability of both GO and MoS_2 decreases significantly when NOM is present with divalent cations in solution. The bridging effect and decrease in the energy barrier help NOM to deposit onto the material surfaces in the presence of divalent cations. Overall, average deposition of NOM and attachment efficiecncy were slightly lower on MoS_2 than GO especially in the case of NOM in Mg^{2+}.

3.5 Interactions of GO and MoS_2 with *E. coli*

The maximum frequency shift during *E. coli* deposition in the presence of 10 mM NaCl is shown in figures 6A, S10 & S11. After 30 min of *E. coli* injection, *E. coli* in Na^+ showed an average frequency shift of 7.39 Hz (Fig. S10) on GO surfaces while the average shift was 5.59 Hz (Fig. S11) on MoS_2 surfaces, indicating that overall deposition of *E. coli* was slightly lower on MoS_2 than GO in this case also. Figure 6B shows that the average attachment efficiencies of *E. coli* in Na^+ were 71% and 62% on GO and MoS_2 surfaces, respectively. However, it has been found the the interaction of *E. coli* with GO and MoS_2 surfaces was not significantly different unlike the interaction of NOM. Nevertheless, low attachment efficiency for GO and MoS_2 indicates an improvement of the antifouling properties of both the surface. Poitras and Tufenkji reported that

QCM-D underestimates the mass adsorbed on the crystal surface for "soft mass" such as bacterial cells.[44] They reported that along with frequency shift, the dissipation shift also changed significantly during *E. coli* deposition. Though the interaction of E. coli is highly surface dependent, in this study, significant dissipation shit was also noticed. The changes in dissipation shift on GO and MoS_2 surfaces were $15.52*10^{-6}$ (Fig. S10) and $12.13*10^{-6}$ (Fig. S11) on average respectively. It is important to report that the increase in dissipation shift during the *E. coli* deposition was much higher than the NOM deposition which indicates that the *E. coli* creates a softer layer than NOM on 2D material surfaces.

E. coli, which are gram negative bacteria, have an outer covering of lipopolysaccharides that impart a strongly negative charge to the surface of the gram negative bacterial cells.[45] We hypothesize that any attachment of *E. coli* to the material surfaces that did occur might be due to extracellular polymeric substances (EPSs).[46, 47] Previously it has been observed that stationary phase cells cultivated in LB media have less negative charge than the exponential phase cells and tend to aggregate more,[48] which may also contribute to the cell attachment on the material surfaces. In another study, it has been reported that *E. coli* MG1655 aggregates more in the stationary phase due to high protein content on free EPS.[49] Overall, MoS_2 performed as good as GO in terms of average deposition and attachment efficiency against *E. coli.*

4. Mechanisms involved in the interaction of foulants on GO and MoS_2 surfaces

4.1 Influence of surface charge and salt bridging

Figures 7 and S13 represent the overall mechanisms in interactions of MoS_2 and GO with NOM and bacteria, respectively. Interaction energy between *E. coli* and GO and MoS_2 in the presence of monovalent ions was calculated using DLVO theory (Supporting Information). The zeta

potential and hydrodynamic size of *E. coli* in 10mM NaCl were -44.2 mV and 2 µm, respectively, under experimental conditions. Result from DLVO theory (Figure S12) suggest that the energy barrier between the *E. coli* and the 2D material surfaces was very high (2000 KT). The high negative surface charge of the 2D materials creates unfavorable conditions for NOM deposition also. However, there was still deposition of the foulants on the material surfaces particularly on GO due to salt bridging. The presence of divalent cations (Ca^{2+} , Mg^{2+}) contributes to the NOM-NOM interaction[50, 51] and may also causes deposition of foulants as Ca^{2+} or Mg^{2+} could work as a linker between NOM and GO or MoS_2. Furthermore, divalent cations can reduce electrostatic and steric effects and influence the interaction of foulants on the material surfaces. [37, 39, 42] Due to the large amount of functional groups, GO is more prone to salt bridging. On the other hand, lack of functional groups on MoS_2 makes the surface unfavorable for salt bridging, which results in sligtly lower attachment of foulants on MoS_2 than GO. Furthermore, the energy barriers between foulants and material surfaces fall at a separation distance of 20-22 nm (secondary minimum) and the interaction energy is not repulsive after that point (Fig S12). In the case of *E. coli*, the secondary minimum starts at 23 nm with the maximum attraction energy of 1.32 KT at 29 nm (Fig. S12). This indicates that the higher energy barrier is not effective beyond that range and other interactions, such as the presence of functional groups and surface roughness, may play the dominant role.

Most of the foulants in nature are negatively charged and thus negatively charged membranes can create electrostatic repulsion between foulants co ions and membranes surface.[52] However, the electrostatic repulsion could be overcome by the foulants due to secondary minimum where hydrogen bond, van dar Waals force dominate. Few recent studies have reported that sometimes charge neutral surfaces perform better as antifouling surfaces.[53, 54]

4.2 Influence of functional groups and surface roughness

NOM contains carboxyl, hydroxyl, and amino functional groups [55-57] and GO contains primarily epoxy, hydroxyl, and carboxyl functional groups (Fig. 2 and S13). [58, 59] NOM molecules have been reported to adsorb on GO via hydrogen bonds, Lewis acid−base, and π-π interactions (Fig. S13).[56] Hydroxyl functional groups of NOM can form hydrogen bonds with oxygen-containing functional groups of GO. [56, 60] On the other hand, lack of functional groups (Fig. 2) on MoS_2 will reduce the interactions of NOM, which was confirmed by the lower attachment of NOM with MoS_2 than GO. However, hydrophobic interactions between the foulants and the MoS_2 may be responsible for foulant deposition on MoS_2 surfaces (Fig. 7). [61] NOM has both hydrophilic and hydrophobic fractions and the hydrophobic humic substances constitute the major NOM fraction. [62] MoS_2 is hydrophobic in nature and can interact with the hydrophobic parts of the foulants. *E. coli* mainly attach to the material surfaces due to the extracellular polymeric substances (EPSs) from their outer surface. EPSs consisting of polysaccharides, proteins and other biopolymers also have functional groups like carboxyl, hydroxyl, amino functional groups on their structures (Fig. 7 & S13). Presence of these functional group help *E. coli* to bind with GO and MoS_2 functionalized surfaces (Fig. 7 & S13). Presence of functional groups in GO forms hydrogen bond with the lipopolysaccharides (LPS) of Gram-negative (*E. coli*) bacteria. [63, 64] Also, physisorbed bulk water on MoS_2 surfaces may form hydrogen bond with the –OH functional groups of polysaccharides.[64] Constituents of EPSs have different patches or domains that can be hydrophobic, hydrophilic, positively or negatively charged nature.[65, 66] Complex structure of those proteins and polysaccharides favor the *E. coli* deposition on both material surfaces. However, deposition of *E. coli* on MoS_2 surface was significantly lower due to lack of functional groups.

In most cases, the foulants showed slightly less attachment to MoS_2 surfaces than to GO surfaces. However, additional mechanisms may also play a role in this difference in antifouling behavior. In particular, surface roughness is an important parameter to consider in any fouling study. The surface roughness of the PLL, GO on PLL and MoS_2 on PLL surfaces used in this study were measured to be 5.1 ± 1.2 nm, 2.5 ± 0.3 nm and 2.4 ± 0.3 nm, respectively. This indicates that the addition of GO and MoS_2 creates a smoother surface than the bare polymer surface. This higher roughness value may contribute to the higher fouling occurring on the bare polymer surface in addition to the contribution of the positive charges on polymer surface. Rough surfaces are more susceptible to fouling as foulants deposit in valleys, making it difficult to remove the foulants by hydrodynamic force. [67, 68] Both the GO and MoS_2 surfaces showed negligible differences in roughness, and thus the functional groups of GO are likely responsible for lower antifouling properties compared to MoS_2.

5. Conclusions

GO has been a research interest for preparing antifouling membranes and surface for long time. Overall, from this study, it was found that MoS_2 performs significantly better than GO under most of the fouling conditions investigated in this study. MoS_2 shows more potential for antifouling applications than GO due to lower interactions with foulants on MoS_2. Better antifouling property of MoS_2 could certainly take over GO for preparation of antifouling surfaces in near future. Ca^{2+} and Mg^{2+} can play a significant role in bridging with foulant molecules and GO and MoS_2 functionalized surfaces. Higher frequency shifts observed in QCM-D suggest that the presence of Ca^{2+} and Mg^{2+} in natural water results in higher deposition of foulants that may impede high water flux and thus the efficiency of the membrane during water filtration. Monovalent ions have less effect on the accumulation of foulants on the material surfaces.

Additionally, *E. coli* showed deposition on both GO and MoS_2 surfaces. *E. coli* also creates a softer layer on the material surfaces than NOM confirmed by the higher dissipation shift change on QCM-D during *E. coli* deposition on GO and MoS_2 surfaces. Results indicate that MoS_2 may be more suitable for antifouling surfaces and membrane applications.

Conflicts of interest

There are no conflicts to declare.

Acknowledgments

This work was supported by a New Faculty Award from Washington State University**.** This work was also supported by the National Science Foundation and the Environmental Protection Agency under Cooperative Agreement Number DBI-1266377.

Supporting Information Available

Additional figures and tables are available free of charge via the Internet at http://pubs.acs.org

Table 1. Average size, zeta potential, mobility and polydispersity index of the GO and MoS_2 dispersions.

Sample name	Average Zeta Potential (mV)	Average Mobility (µmcm/Vs)	Average Size (d.nm)	PdI
GO in MQ water	-41.33±0.5	-3.24±0.04	385.3±7.58	0.49±0.05
MoS_2 in MQ water	-40.34±0.76	-3.16±0.06	153.5±1.67	0.22±0.01

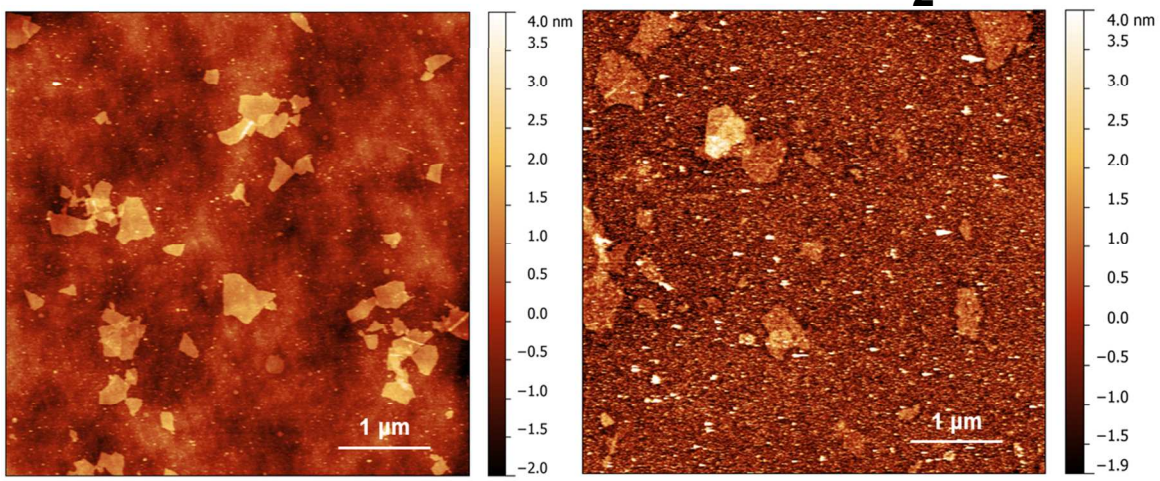

Figure 1. AFM images of GO and MoS_2 on SiO_2. The flakes are mainly monolayer or bilayer with a wide range of lateral sizes.

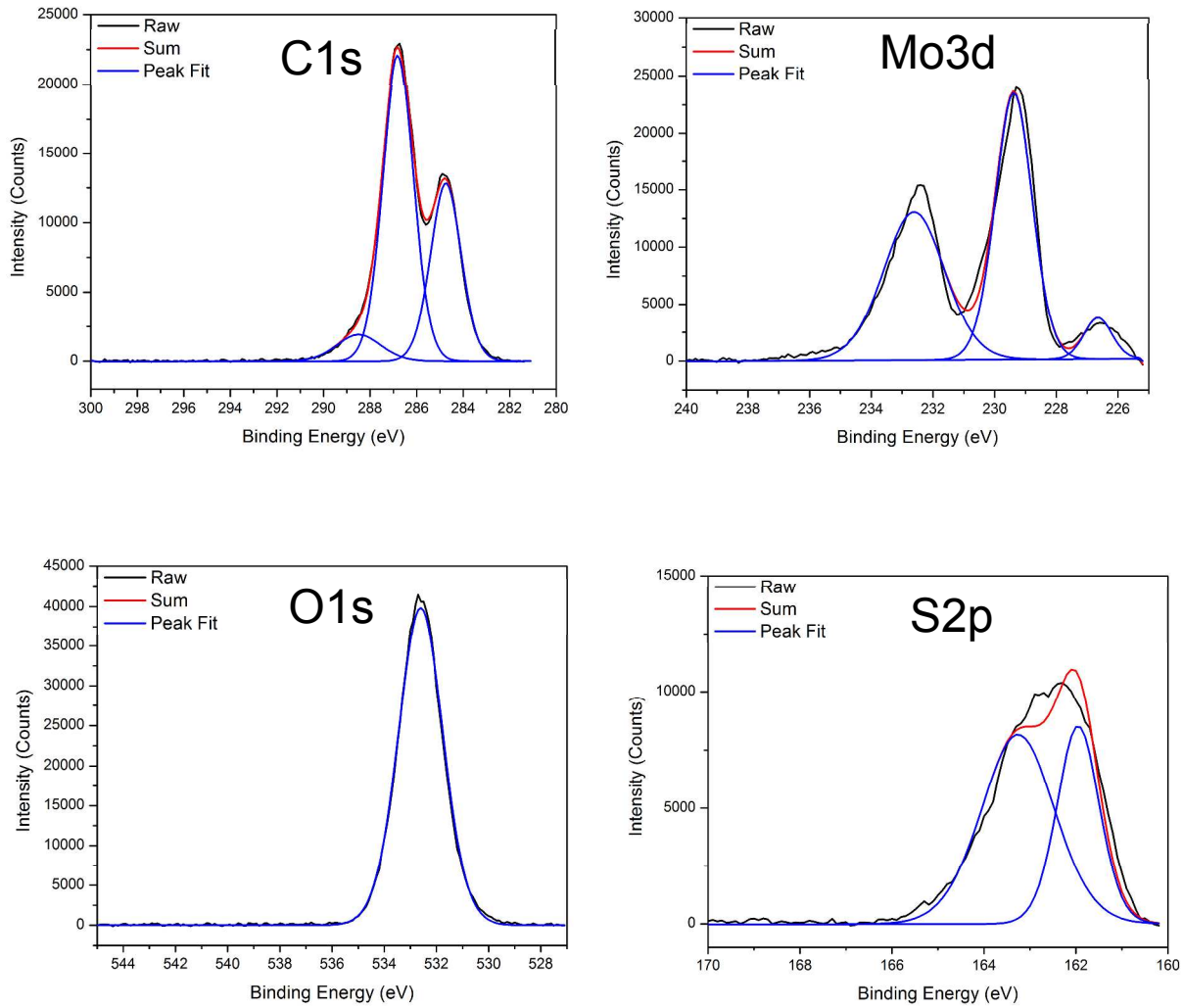

Figure 2: XPS spectra of GO and MoS_2. Three convoluted peaks corresponding to C-C (~284.8 eV), C-O (~286.8 eV) and O-C=O (288.5 eV) in GO C1s spectra confirms presence of oxygen containing functional groups on GO structure. XPS spectra of MoS_2 did not show any indication of oxidation. The characteristic 3 peaks in the Mo3d scan corresponding to the Mo3d 3/2 (~232.5 eV), Mo3d 5/2 (~229 eV) and S2s (~226.5 eV) and the characteristic doublet peak in the S2p spectrum were found on XPS of MoS_2.

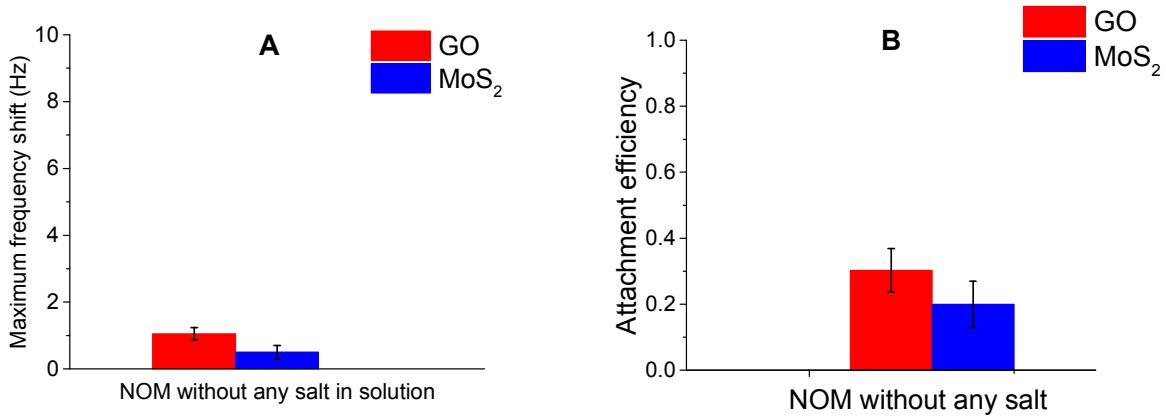

Figure 3. (A) Maximum frequency shift of GO and MoS_2 surfaces against NOM without any salts on QCM-D. MoS_2 showed the least NOM attachment on its surface. Error bars represent the standard deviation of the experimental results (98% confidence interval). (B) Attachment efficiency of NOM on both of the surfaces (93% confidence interval).

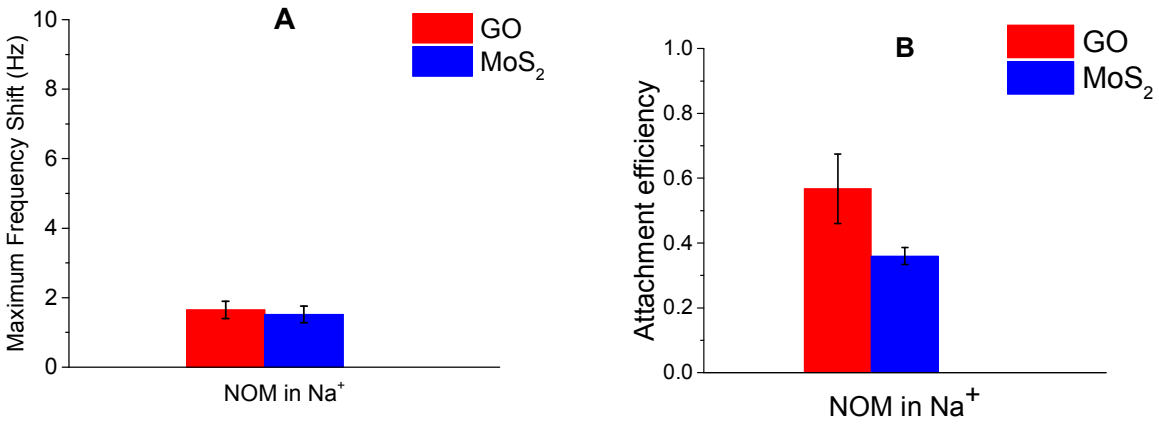

Figure 4. (A) Maximum frequency shift of GO and MoS_2 surfaces against NOM in presence of 10 mM NaCl on QCM-D. NOM in 10 mM NaCl showing slightly higher frequency shifts on both the material surfaces indicated higher deposition compared to NOM with any salts. Error bars represent the standard deviation of the experimental results conducted on different cells of QCM-D (<90% confidence interval). (B) Attachment efficiency of NOM in 10 mM NaCl on GO and MoS_2 (99% confidence interval).

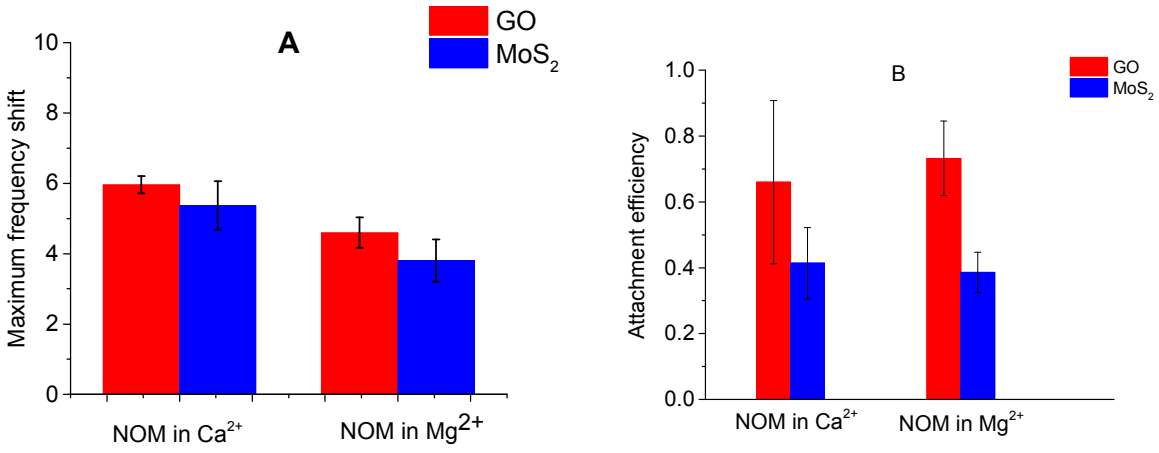

Figure 5. (A) Maximum frequency shift of GO and MoS_2 surfaces against NOM with the presence of 0.5 mM divalent cations on QCM-D (93% confidence interval for $CaCl_2$ & 99% confidence interval for $MgCl_2$). (B) Attachment efficiency of NOM in 0.5 mM $CaCl_2$ (<90% confidence interval) and 0.5 mM $MgCl_2$ (100% confidence interval)on both GO and MoS_2 surfaces. Higher frequency shift and attachment efficiency indicate higher and faster accumulation of NOM on the material surfaces in the presence of divalent ions.

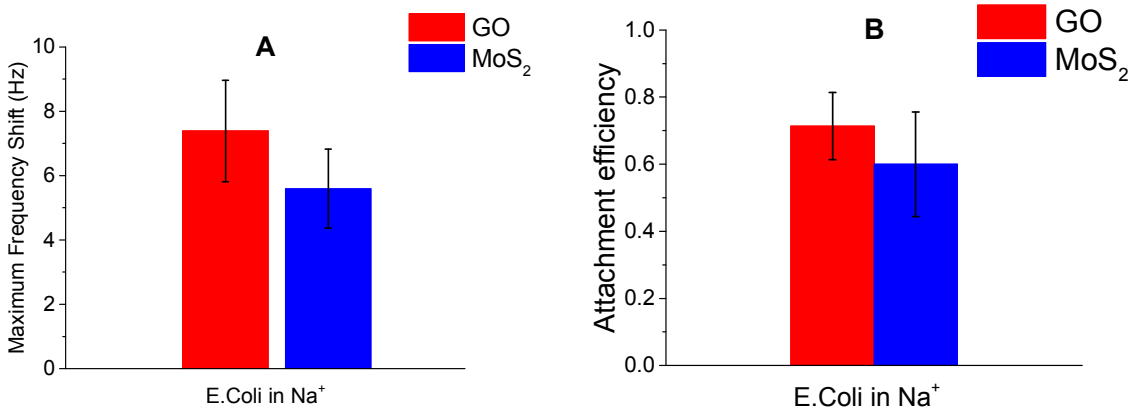

Figure 6. (A) Maximum frequency shift of *E. coli* in 10 mM NaCl on both GO and MoS_2 surfaces (90% confidence interval). (B) Attachment efficiency of *E. coli* in 10 mM NaCl on both GO and MoS_2 surfaces (<90% confidence interval).

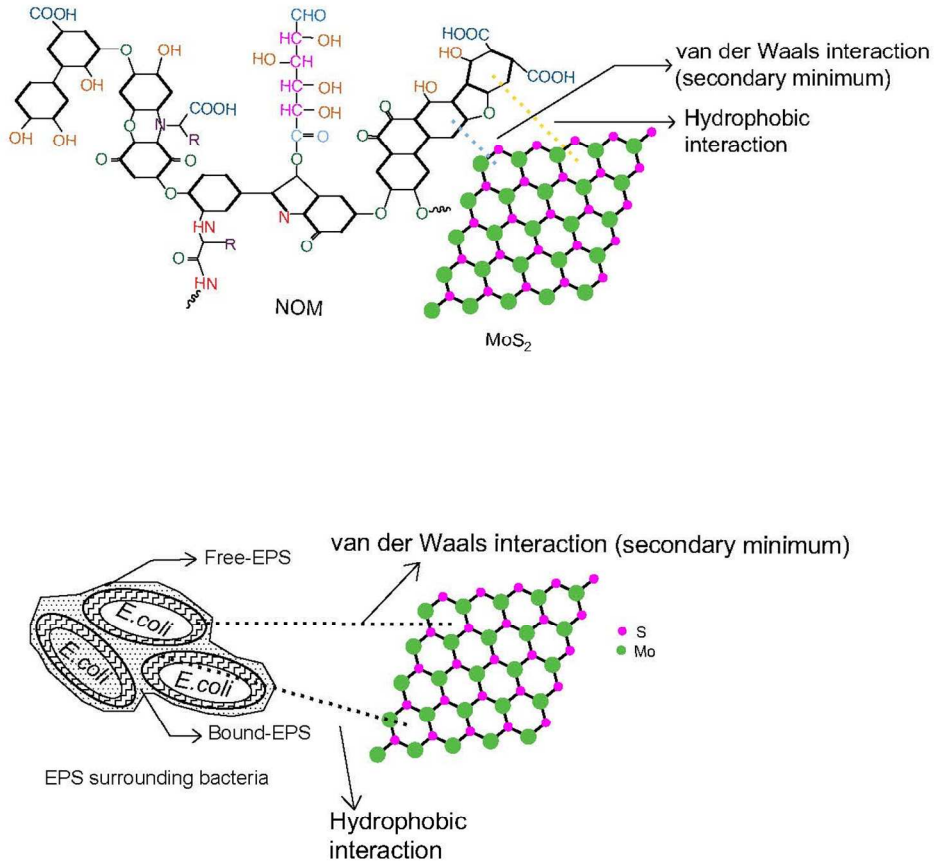

Figure 7. Mechanisms of interactions of MoS_2 with NOM and *E. coli*. Absence of functional groups in MoS_2 structure makes unfavorable condition for foulants deposition. Van der Waals interactions and hydrophobic interactions have been reported to form between NOM and MoS_2. Sticky polymeric substances from *E. coli* show high affinities to the MoS_2 surface.

References

1. Y. Wu, M. Xu, X. Chen, S. Yang, H. Wu, J. Pan and X. Xiong, CTAB-assisted synthesis of novel ultrathin MoSe 2 nanosheets perpendicular to graphene for the adsorption and photodegradation of organic dyes under visible light, *Nanoscale*, 2016, **8**, 440-450.
2. M. Hu and B. Mi, Enabling graphene oxide nanosheets as water separation membranes, *Environmental science & technology*, 2013, **47**, 3715-3723.
3. Z. Cai, A. D. Dwivedi, W.-N. Lee, X. Zhao, W. Liu, M. Sillanpää, D. Zhao, C.-H. Huang and J. Fu, Application of nanotechnologies for removing pharmaceutically active compounds from water: development and future trends, *Environmental Science: Nano*, 2018, **5**, 27-47.
4. J. Chen, H. Peng, X. Wang, F. Shao, Z. Yuan and H. Han, Graphene oxide exhibits broad-spectrum antimicrobial activity against bacterial phytopathogens and fungal conidia by intertwining and membrane perturbation, *Nanoscale*, 2014, **6**, 1879-1889.
5. O. Akhavan and E. Ghaderi, Toxicity of Graphene and Graphene Oxide Nanowalls Against Bacteria, *ACS Nano*, 2010, **4**, 5731-5736.
6. S. Krishnan, C. J. Weinman and C. K. Ober, Advances in polymers for anti-biofouling surfaces, *Journal of Materials Chemistry*, 2008, **18**, 3405-3413.
7. J. Lee, H.-R. Chae, Y. J. Won, K. Lee, C.-H. Lee, H. H. Lee, I.-C. Kim and J.-m. Lee, Graphene oxide nanoplatelets composite membrane with hydrophilic and antifouling properties for wastewater treatment, *Journal of Membrane Science*, 2013, **448**, 223-230.
8. D. Lembke, S. Bertolazzi and A. Kis, Single-layer MoS2 electronics, *Accounts of chemical research*, 2015, **48**, 100-110.

9. Z. Wang and B. Mi, Environmental Applications of 2D Molybdenum Disulfide (MoS2) Nanosheets, *Environmental Science & Technology*, 2017, **51**, 8229-8244.

10. T. I. Kim, B. Kwon, J. Yoon, I.-J. Park, G. S. Bang, Y. Park, Y.-S. Seo and S.-Y. Choi, Antibacterial Activities of Graphene Oxide–Molybdenum Disulfide Nanocomposite Films, *ACS Applied Materials & Interfaces*, 2017, **9**, 7908-7917.

11. M. Chhowalla and G. A. J. Amaratunga, Thin films of fullerene-like MoS2 nanoparticles with ultra-low friction and wear, *Nature*, 2000, **407**, 164-167.

12. Q. H. Wang, K. Kalantar-Zadeh, A. Kis, J. N. Coleman and M. S. Strano, *Nat. Nanotechnol.*, 2012, **7**, 699.

13. M. Heiranian, A. B. Farimani and N. R. Aluru, Water desalination with a single-layer MoS2 nanopore, *Nat Commun*, 2015, **6**.

14. K. R. Zodrow, E. Bar-Zeev, M. J. Giannetto and M. Elimelech, Biofouling and Microbial Communities in Membrane Distillation and Reverse Osmosis, *Environmental Science & Technology*, 2014, **48**, 13155-13164.

15. Q. Li and M. Elimelech, Organic Fouling and Chemical Cleaning of Nanofiltration Membranes: Measurements and Mechanisms, *Environmental Science & Technology*, 2004, **38**, 4683-4693.

16. X. Zhu and M. Elimelech, Colloidal Fouling of Reverse Osmosis Membranes: Measurements and Fouling Mechanisms, *Environmental Science & Technology*, 1997, **31**, 3654-3662.

17. K. Listiarini, W. Chun, D. D. Sun and J. O. Leckie, Fouling mechanism and resistance analyses of systems containing sodium alginate, calcium, alum and their combination in

dead-end fouling of nanofiltration membranes, *Journal of Membrane Science*, 2009, **344**, 244-251.

18. T. Nguyen, F. A. Roddick and L. Fan, Biofouling of water treatment membranes: a review of the underlying causes, monitoring techniques and control measures, *Membranes*, 2012, **2**, 804-840.

19. A. Ruiz-García, N. Melián-Martel and I. Nuez, A Critical Review on Predicting Fouling in RO Desalination, 2017.

20. E. Almeida, T. C. Diamantino and O. de Sousa, Marine paints: the particular case of antifouling paints, *Progress in Organic Coatings*, 2007, **59**, 2-20.

21. D. Crisp, The role of the biologist in antifouling research, *RF Acker et al., Proc. of the Third ICMCF, Northwestern University Press, Evanston, IL*, 1973, 88.

22. M. E. Callow and J. A. Callow, Marine biofouling: a sticky problem, *Biologist*, 2002, **49**, 1-5.

23. H. Zhang and M. Chiao, Anti-fouling Coatings of Poly(dimethylsiloxane) Devices for Biological and Biomedical Applications, *Journal of Medical and Biological Engineering*, 2015, **35**, 143-155.

24. J. Bohnert, T. Horbett, B. a. Ratner and F. Royce, Adsorption of proteins from artificial tear solutions to contact lens materials, *Investigative ophthalmology & visual science*, 1988, **29**, 362-373.

25. J. C. Crittenden, R. R. Trussell, D. W. Hand, K. J. Howe and G. Tchobanoglous, *MWH's Water Treatment: Principles and Design*, Wiley, 2012.

26. W. Hu, C. Peng, W. Luo, M. Lv, X. Li, D. Li, Q. Huang and C. Fan, Graphene-Based Antibacterial Paper, *ACS Nano*, 2010, **4**, 4317-4323.

27. A. Adout, S. Kang, A. Asatekin, A. M. Mayes and M. Elimelech, Ultrafiltration Membranes Incorporating Amphiphilic Comb Copolymer Additives Prevent Irreversible Adhesion of Bacteria, *Environmental Science & Technology*, 2010, **44**, 2406-2411.

28. M. C. Duch, G. R. S. Budinger, Y. T. Liang, S. Soberanes, D. Urich, S. E. Chiarella, L. A. Campochiaro, A. Gonzalez, N. S. Chandel, M. C. Hersam and G. M. Mutlu, Minimizing Oxidation and Stable Nanoscale Dispersion Improves the Biocompatibility of Graphene in the Lung, *Nano Letters*, 2011, **11**, 5201-5207.

29. I. Chowdhury, M. C. Duch, N. D. Mansukhani, M. C. Hersam and D. Bouchard, Colloidal Properties and Stability of Graphene Oxide Nanomaterials in the Aquatic Environment, *Environmental Science & Technology*, 2013, **47**, 6288-6296.

30. J. D. Lanphere, C. J. Luth, L. M. Guiney, N. D. Mansukhani, M. C. Hersam and S. L. Walker, Fate and Transport of Molybdenum Disulfide Nanomaterials in Sand Columns, *Environmental Engineering Science*, 2015, **32**, 163-173.

31. W.-C. Hou, I. Chowdhury, D. G. Goodwin, W. M. Henderson, D. H. Fairbrother, D. Bouchard and R. G. Zepp, Photochemical Transformation of Graphene Oxide in Sunlight, *Environmental Science & Technology*, 2015, **49**, 3435-3443.

32. M. R. Esfahani, E. M. Languri and M. R. Nunna, Effect of particle size and viscosity on thermal conductivity enhancement of graphene oxide nanofluid, *International Communications in Heat and Mass Transfer*, 2016, **76**, 308-315.

33. M. Elimelech, J. Gregory, X. Jia and R. A. F. Williams, *Particle Deposition and Aggregation: Measurement, Modelling and Simulation*, Elsevier Science, 2013.

34. D. Bouchard, X. Ma and C. Isaacson, Colloidal Properties of Aqueous Fullerenes: Isoelectric Points and Aggregation Kinetics of C60 and C60 Derivatives, *Environmental Science & Technology*, 2009, **43**, 6597-6603.

35. A. A. Taylor, I. Chowdhury, A. S. Gong, D. M. Cwiertny and S. L. Walker, Deposition and disinfection of Escherichia coli O157:H7 on naturally occurring photoactive materials in a parallel plate chamber, *Environmental Science: Processes & Impacts*, 2014, **16**, 194-202.

36. I. Chowdhury, M. C. Duch, N. D. Mansukhani, M. C. Hersam and D. Bouchard, Deposition and Release of Graphene Oxide Nanomaterials Using a Quartz Crystal Microbalance, *Environmental Science & Technology*, 2014, **48**, 961-969.

37. K. L. Chen and M. Elimelech, Interaction of Fullerene (C60) Nanoparticles with Humic Acid and Alginate Coated Silica Surfaces: Measurements, Mechanisms, and Environmental Implications, *Environ. Sci. Technol.*, 2008, **42**, 7607.

38. K. L. Chen and M. Elimelech, Aggregation and deposition kinetics of fullerene (C60) nanoparticles, *Langmuir*, 2006, **22**, 10994.

39. I. Chowdhury, M. C. Duch, N. D. Mansukhani, M. C. Hersam and D. Bouchard, Interactions of Graphene Oxide Nanomaterials with Natural Organic Matter and Metal Oxide Surfaces, *Environmental Science & Technology*, 2014, **48**, 9382-9390.

40. J. Buffle, K. J. Wilkinson, S. Stoll, M. Filella and J. Zhang, A generalized description of aquatic colloidal interactions: the three-colloidal component approach, *Environmental Science & Technology*, 1998, **32**, 2887-2899.

41. X. Chang and D. C. Bouchard, Multiwalled Carbon Nanotube Deposition on Model Environmental Surfaces, *Environmental Science & Technology*, 2013, **47**, 10372-10380.

42. W. S. Ang and M. Elimelech, Protein (BSA) fouling of reverse osmosis membranes: Implications for wastewater reclamation, *Journal of Membrane Science*, 2007, **296**, 83-92.

43. A. C. Ribou, J. Vigo, P. Viallet and J. M. Salmon, Interaction of a protein, BSA, and a fluorescent probe, Mag-Indo-1, influence of EDTA and calcium on the equilibrium, *Biophysical Chemistry*, 1999, **81**, 179-189.

44. C. Poitras and N. Tufenkji, A QCM-D-based biosensor for E. coli O157:H7 highlighting the relevance of the dissipation slope as a transduction signal, *Biosens. Bioelectron.*, 2009, **24**, 2137.

45. T. J. Silhavy, D. Kahne and S. Walker, The Bacterial Cell Envelope, *Cold Spring Harbor Perspectives in Biology*, 2010, **2**, a000414.

46. L. V. Evans, *Biofilms: Recent Advances in their Study and Control*, Taylor & Francis, 2003.

47. G.-P. Sheng, H.-Q. Yu and X.-Y. Li, Extracellular polymeric substances (EPS) of microbial aggregates in biological wastewater treatment systems: A review, *Biotechnology Advances*, 2010, **28**, 882-894.

48. K. Eboigbodin, J. Newton, A. Routh and C. Biggs, Bacterial quorum sensing and cell surface electrokinetic properties, *Applied microbiology and biotechnology*, 2006, **73**, 669-675.

49. K. E. Eboigbodin and C. A. Biggs, Characterization of the Extracellular Polymeric Substances Produced by Escherichia coli Using Infrared Spectroscopic, Proteomic, and Aggregation Studies, *Biomacromolecules*, 2008, **9**, 686-695.

50. S. Hong and M. Elimelech, Chemical and physical aspects of natural organic matter (NOM) fouling of nanofiltration membranes, *Journal of Membrane Science*, 1997, **132**, 159-181.

51. M. Baalousha, M. Motelica-Heino and P. L. Coustumer, Conformation and size of humic substances: Effects of major cation concentration and type, pH, salinity, and residence time, *Colloids and Surfaces A: Physicochemical and Engineering Aspects*, 2006, **272**, 48-55.

52. A. Ahmadi, O. Qanati, M. S. Seyed Dorraji, M. H. Rasoulifard and V. Vatanpour, Investigation of antifouling performance a novel nanofibrous S-PVDF/PVDF and S-PVDF/PVDF/GO membranes against negatively charged oily foulants, *Journal of Membrane Science*, 2017, **536**, 86-97.

53. D. H. Seo, S. Pineda, Y. C. Woo, M. Xie, A. T. Murdock, E. Y. M. Ang, Y. Jiao, M. J. Park, S. I. Lim, M. Lawn, F. F. Borghi, Z. J. Han, S. Gray, G. Millar, A. Du, H. K. Shon, T. Y. Ng and K. Ostrikov, Anti-fouling graphene-based membranes for effective water desalination, *Nature Communications*, 2018, **9**, 683.

54. H. Yamamura, K. Kimura, T. Okajima, H. Tokumoto and Y. Watanabe, Affinity of Functional Groups for Membrane Surfaces: Implications for Physically Irreversible Fouling, *Environmental Science & Technology*, 2008, **42**, 5310-5315.

55. R. Sutton and G. Sposito, Molecular Structure in Soil Humic Substances: The New View, *Environmental Science & Technology*, 2005, **39**, 9009-9015.

56. T. Hartono, S. Wang, Q. Ma and Z. Zhu, Layer structured graphite oxide as a novel adsorbent for humic acid removal from aqueous solution, *Journal of Colloid and Interface Science*, 2009, **333**, 114-119.

57. M. Baalousha, M. Motelica-Heino and P. L. Coustumer, Conformation and size of humic substances: Effects of major cation concentration and type, pH, salinity, and residence time, *Colloids and Surfaces A: Physicochemical and Engineering Aspects*, 2006, **272**, 48-55.

58. W. Gao, L. B. Alemany, L. Ci and P. M. Ajayan, New insights into the structure and reduction of graphite oxide, *Nat Chem*, 2009, **1**, 403-408.

59. D. R. Dreyer, S. Park, C. W. Bielawski and R. S. Ruoff, The chemistry of graphene oxide, *Chemical Society Reviews*, 2010, **39**, 228-240.

60. D. Chen, H. Feng and J. Li, Graphene Oxide: Preparation, Functionalization, and Electrochemical Applications, *Chemical Reviews*, 2012, **112**, 6027-6053.

61. X. Gao, X. Wang, X. Ouyang and C. Wen, Flexible superhydrophobic and superoleophilic MoS2 sponge for highly efficient oil-water separation, *Scientific reports*, 2016, **6**, 27207.

62. Y. Penru, F. X. Simon, A. R. Guastalli, S. Esplugas, J. Llorens and S. Baig, Characterization of natural organic matter from Mediterranean coastal seawater, *Journal of water supply: Research and Technology-AQUA*, 2013, **62**, 42-51.

63. B. A. Jucker, H. Harms and A. J. B. Zehnder, Polymer interactions between five gram-negative bacteria and glass investigated using LPS micelles and vesicles as model systems, *Colloids and Surfaces B: Biointerfaces*, 1998, **11**, 33-45.

64. B. A. Jucker, H. Harms, S. J. Hug and A. J. B. Zehnder, Adsorption of bacterial surface polysaccharides on mineral oxides is mediated by hydrogen bonds, *Colloids and Surfaces B: Biointerfaces*, 1997, **9**, 331-343.

65. D. Asthagiri and A. M. Lenhoff, Influence of Structural Details in Modeling Electrostatically Driven Protein Adsorption, *Langmuir*, 1997, **13**, 6761-6768.

66. A. Wittemann and M. Ballauff, Interaction of proteins with linear polyelectrolytes and spherical polyelectrolyte brushes in aqueous solution, *Physical Chemistry Chemical Physics*, 2006, **8**, 5269-5275.

67. N. Shahkaramipour, T. N. Tran, S. Ramanan and H. Lin, Membranes with Surface-Enhanced Antifouling Properties for Water Purification, *Membranes*, 2017, **7**, 13.

68. E. M. Vrijenhoek, S. Hong and M. Elimelech, Influence of membrane surface properties on initial rate of colloidal fouling of reverse osmosis and nanofiltration membranes, *Journal of Membrane Science*, 2001, **188**, 115-128.

TOC Art

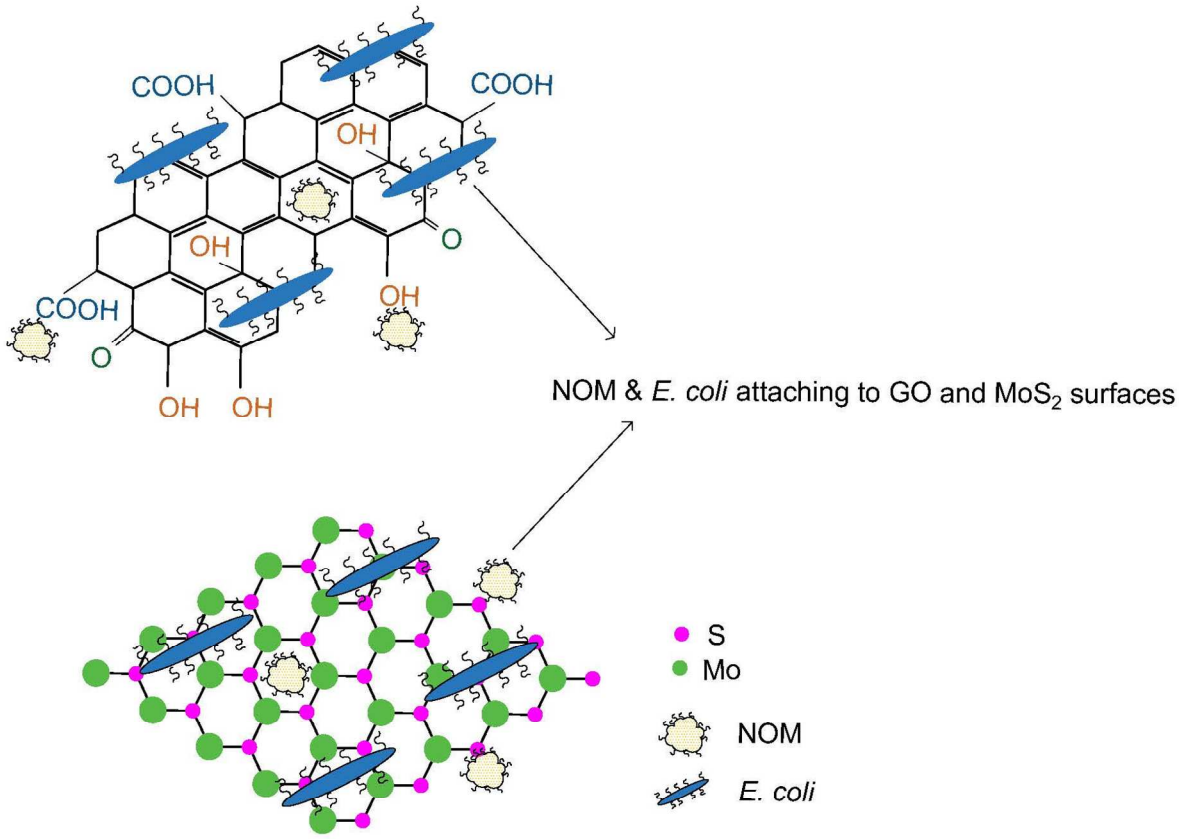
COOH
COOH
OH
O
OH
COOH
O
OH
OH
OH
NOM & E. coli attaching to GO and MoS2 surfaces
S
Mo
NOM
E. coli